Stratigraphy, composition and provenance of argillaceous marls from the Calcare di Base Formation, Rossano Basin (northeastern Calabria)

FRANCESCO PERRI†, ROCCO DOMINICI & SALVATORE CRITELLI

Dipartimento di Biologia, Ecologia e Scienze della Terra, Università della Calabria, 87036 Arcavacata di Rende (CS), Italy

Abstract – The Calcare di Base Formation is a part of the Rossano Basin characterizing the Foreland Basin System of northeastern Calabria. Messinian argillaceous marls from the Calcare di Base Formation have been studied to characterize the sedimentary evolution of this formation during the post-orogenic phases of the Calabria–Peloritani Arc. The mineralogical assemblage of the argillaceous marls is dominated by phyllosilicates (illite, chlorite, illite/smectite mixed layers and traces of kaolinite), carbonate minerals (calcite, aragonite and dolomite), quartz and traces of feldspars (both K-feldspars and plagioclase), gypsum and celestine. The palaeoweathering index records changes at the source, reflecting variations in the tectonic regime as shown in the A–CN–K plot, where the studied samples describe a trend typical of a source area in which active tectonism allows erosion of all zones within weathering profiles developed on source rocks. The studied samples are derived from an environment in which non-steady-state weathering conditions prevailed. This trend could record deformational events that affected the Mediterranean area during the Miocene. The Th/Sc versus Zr/Sc ratios and Al–Zr–Ti plot suggest that the samples likely record a recycling effect from their basement rocks. The geochemical proxies of these samples suggest a provenance from a mainly felsic source. The Messinian argillaceous marls record that deposition probably occurred in a semi-closed marine environment mainly subject to hypersalinity with local episodes of meteoric water influx, during a period characterized by persistent dry and warm/arid conditions alternating with relatively wet conditions.

Keywords: Calcare di Base, Messinian, provenance, argillaceous marls, Rossano Basin, composition.

1. Introduction

During late Miocene time, the Mediterranean region was affected by the Messinian Salinity Crisis, one of the greatest evaporitic events in Earth's history. This crisis was characterized by a combination of tectonic processes (which led to a reduction in the exchange of water between the Mediterranean Sea and the Atlantic Ocean) and palaeoclimate conditions (a regional dry and warm climate) (Fauquette *et al.* 2006; Rouchy & Caruso, 2006; Di Stefano *et al.* 2010; Mongelli *et al.* 2012 and references therein). Different basin scenarios have been hypothesized to explain the origin of the Messinian evaporites: a deep desiccated basin model, shallow-water desiccated basin model or deep non-desiccated basin model (Hsü, Ryan & Cita, 1973; Nesteroff, 1973; Selli, 1973), or the newer scenario proposed by CIESM (2008) composed of three stages. The first stage (5.96–5.6 Ma) is characterized by the onset of the Messinian Salinity Crisis and by the deposition of the so-called 'Lower Evaporites' (selenite in shallow basins and the Tripoli Formation). The second stage (5.6–5.55 Ma) is recorded by a relative sea-level drop and erosion of the evaporitic basins. Finally, the third stage (5.55–5.33 Ma) is characterized by clastic

and evaporitic sedimentation ('Upper Evaporites') containing brackish to fresh-water faunas.

The 'Calcare di Base' is a lithostratigraphic unit composed of carbonate, marls and locally gypsum. The unit was formed during the Messinian Salinity Crisis and it crops out mainly in Sicily and Calabria. Its genesis and spatio-temporal distribution is still debated.

It is the first product of the Messinian evaporitic suite (Ogniben, 1957). This formation has been interpreted either as an evaporitic and/or microbial deposit (Decima, Mckenzie & Schreiber, 1988; Barone *et al.* 2006; Guido *et al.* 2007; Caracciolo *et al.* 2013). It grades laterally into primary selenite of the Lower Gypsum Unit (Roveri *et al.* 2008*a*,*b*) above the lower Messinian Tripoli Formation or as a product of *in situ* collapse due to dissolution of intervening halite or gypsum beds (Pedley & Grasso, 1993) laterally equivalent to primary selenite (Garcia-Veigas *et al.* 1995; Rouchy & Caruso, 2006). There are three main types of limestone deposits commonly included in the Calcare di Base (e.g. Manzi *et al.* 2010): (i) sulfur-bearing limestones which were derived from post-depositional bacterial sulfate reduction (Dessau, Gonfi Antini & Tongiorgi, 1959) (Calcare di Base-1); (ii) interbedded dolostones, sapropels and diatomites usually found at the top or above the Tripoli Formation (Calcare di Base-2); (iii) micritic limestones of evaporative and/or bacterial

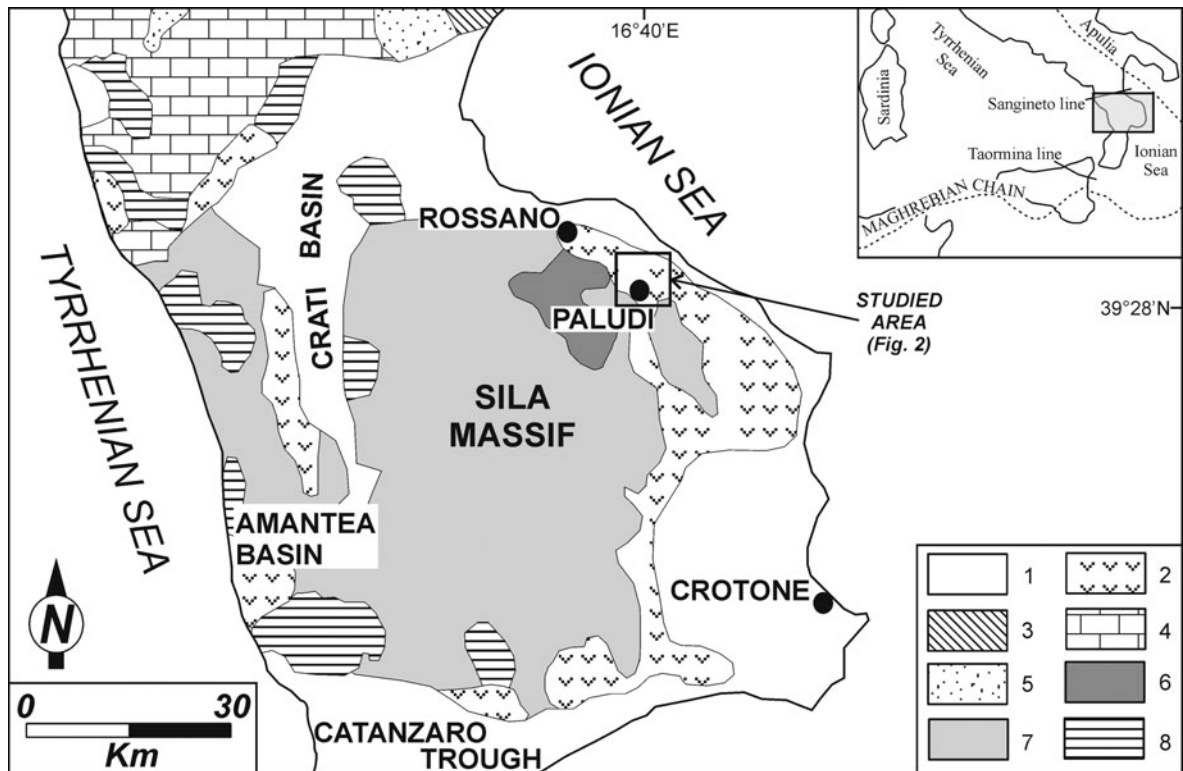†Author for correspondence: francesco.perri@unical.it

Figure 1. Simplified geological map of the central-northern sector of the Calabria–Peloritani Arc with location of the mentioned basins and sites. 1 – Pliocene to Holocene sediments, and volcanic and volcaniclastic rocks; 2 – Upper Tortonian to Messinian clastic rocks and evaporites; 3 – Cilento Group (middle Miocene); 4 – San Donato, Verbicaro and Pollino units (Triassic to Miocene); 5 – Liguride Complex (Upper Jurassic to Upper Oligocene); 6 – Longobucco and Caloveto groups (Lower Jurassic to Lower Cretaceous) and Paludi Formation (Upper Oligocene); 7 – Sila, Castagna and Bagni basement units (Palaeozoic); 8 – Malvito, Diamante–Terranova, Gimigliano ophiolitiferous units (Upper Jurassic to Lower Cretaceous).

origin occurring as resedimented deposits, commonly brecciated, forming metre-thick beds associated with clastic gypsum (Calcare di Base-3).

The Calcare di Base have been recognized in the Rossano, Crotone, Catanzaro Trough, Crati and Amantea basins, and along the Tyrrhenian piedmont area (e.g. Critelli, 1999; Barone *et al.* 2008; Cianflone & Dominici, 2011; Cianflone, Dominici & Sonnino, 2012; Caracciolo *et al.* 2013) (Fig. 1). In the north-eastern Calabrian Foreland Basin, the Calcare di Base forms tabular bodies up to 45 m thick made up of carbonates interbedded with argillaceous marls (e.g. Barone *et al.* 2006, 2008).

In the Rossano Basin, the lithostratigraphic unit of the Calcare di Base has been interpreted to have formed by microbial activity (Guido *et al.* 2007), although Manzi *et al.* (2010) interpreted the same outcrop as originating from gravity flows redepositing unconsolidated limestones. Barone *et al.* (2008) described the Calcare di Base as a 0–45 m thick lithostratigraphic unit characterized by massive and brecciated (with gypsum and halite pseudomorphs) limestone facies interbedded, in some areas, with 10–60 cm thick beds of massive and laminar argillaceous marls. The latter authors suggested an evaporitic and microbial origin followed by subaerial exposure, erosion and karstification producing a strong increase in sedimentary detritus (Barone *et al.* 2006, 2008).

The aim of this paper is to contribute to the debate on the origin of the Calcare di Base using a multidisciplinary study of facies analysis and geochemical and mineralogical tools on the argillaceous marls of the Rossano Basin.

The chemical and mineralogical composition of sediments provide important clues regarding palaeoenvironmental conditions at the time of deposition, including the nature of palaeoweathering and palaeoredox conditions, which yield insights into the palaeoclimate (e.g. Nesbitt & Young, 1982; Wronkiewicz & Condie, 1989; Algeo & Maynard, 2004; Peltola *et al.* 2008). The mineralogy and chemistry of clastic sedimentary rocks is affected by factors such as rock characteristics, chemical weathering, sorting processes during transport and sedimentation, and post-depositional diagenetic reactions (McLennan, Hemming & Hanson, 1993). Furthermore, geochemical proxies provide information on the parental affinity and source area(s) of clastic sediments (e.g. Fedo, Nesbitt & Young, 1995; Mongelli *et al.* 2006, 2012; Critelli *et al.* 2008; Perri *et al.* 2008, 2011, 2012*a*,*b*, 2013; Zaghloul *et al.* 2010; Caracciolo *et al.* 2011; Perri, Muto & Belviso, 2011; Perri, 2014).

2. Geological settings

The Rossano Basin represents the southern sector of the Italian Foreland Basin System located on
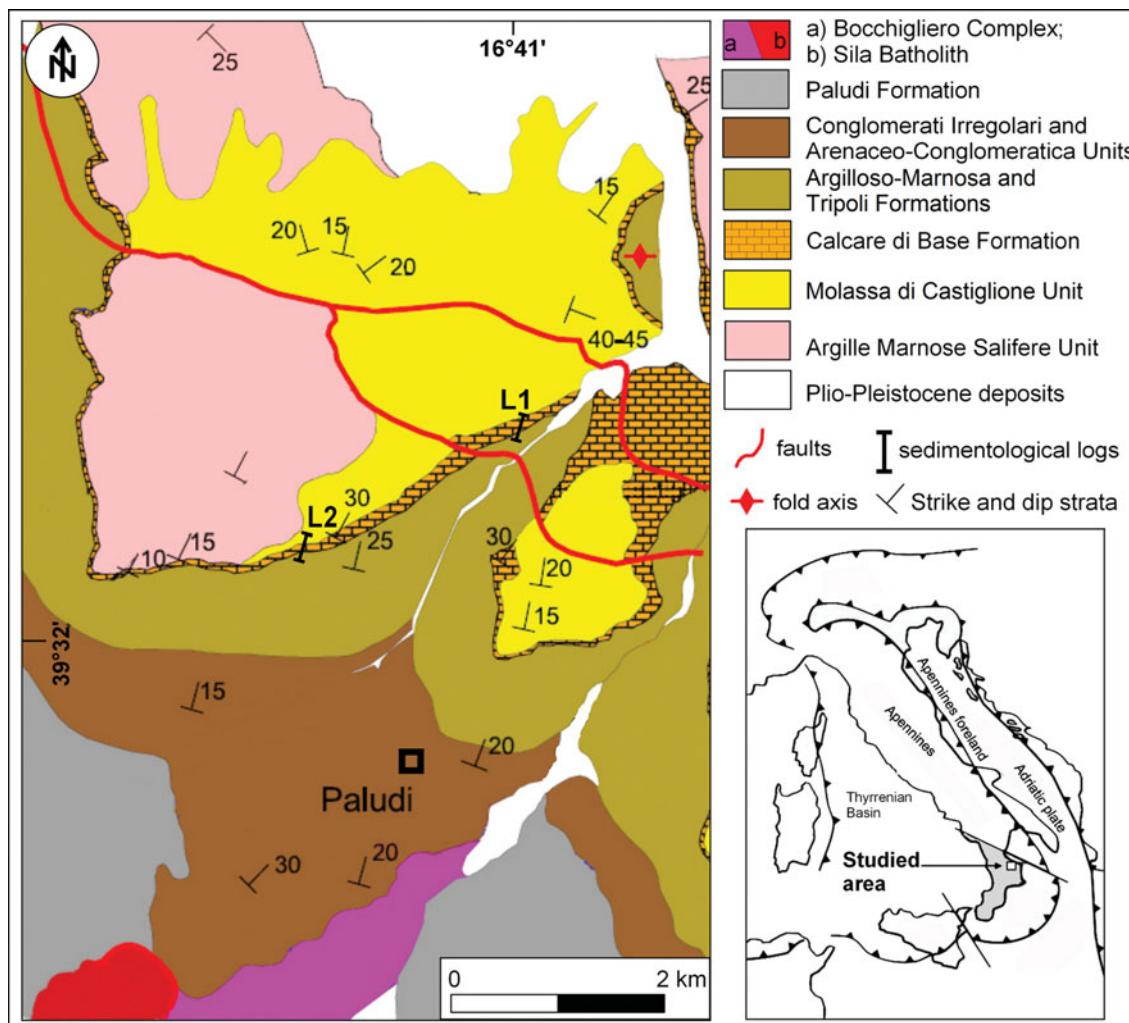
Figure 2. (Colour online) Geological sketch map of the Rossano Basin (northeastern Calabria). L1 and L2 are the sedimentological logs shown in Figure 4.

the northeastern margin of the Calabria–Peloritani Arc. The Calabria–Peloritani Arc represents a fault-bounded exotic terrane connecting the NW–SE-trending southern Apennines with the E–W-trending Sicilian Maghrebids (Critelli & Le Pera, 1995, 1998; Critelli, 1999; Bonardi *et al.* 2001 and references therein). It is made up both of units involving pre-Alpine basements made of continental crust crystalline rocks and covered by Meso-Cenozoic sediments, as well as by ophiolitic units, some of them recording high-pressure/low-temperature Alpine metamorphism and a pre-Miocene tectonism.

The Rossano Basin is the inland portion of a larger Neogene to Quaternary basinal area including the entire Ionian Calabrian continental margin (the Crotone–Spartivento Basin). It was filled with an upper Serravallian to middle Pleistocene continental to deep-marine succession (Roda, 1964, 1967; Critelli, 1999; Van Dijk *et al.* 2000, Barone *et al.* 2008; Zecchin *et al.* 2012, 2013a,b; Tripodi, Muto & Critelli, 2013) that was a tectonically active basin up to the present (e.g. Zecchin *et al.* 2011; Perri *et al.* 2012b).

2.a. Stratigraphy of the Rossano Basin

The base of the Rossano Basin is characterized by transgressive sediments of Serravallian?–Tortonian age that unconformably overlie the lower Miocene Paludi Formation and its underlying low-grade metamorphic (Bocchigliero Complex) and plutonic rocks (Sila Batholith) (e.g. Barone *et al.* 2008; Bonardi *et al.* 2005) (Fig. 2).

The onset of sedimentation included alluvial conglomerates (Conglomerati Irregolari: Roda, 1964), which are overlain by a nearshore succession consisting of sandstones and fossiliferous sandstones (Arenaceo–Conglomeratica Unit). The succession in turn passes upwards into deeper-water sediments (Argilloso–Marnosa Formation) characterized by an alternation of decimetric indurated dark clay and light greyish or light blue marl whose origin is related, at least in its upper part, to astronomical cyclicity (Barone *et al.* 2008). During late Tortonian time, the Agilloso–Marnosa Formation received huge volumes of olistostromes eroded from the 'Argille Scagliose Formation' (Sicilide Complex: Ogniben, 1955, 1962). These rocks
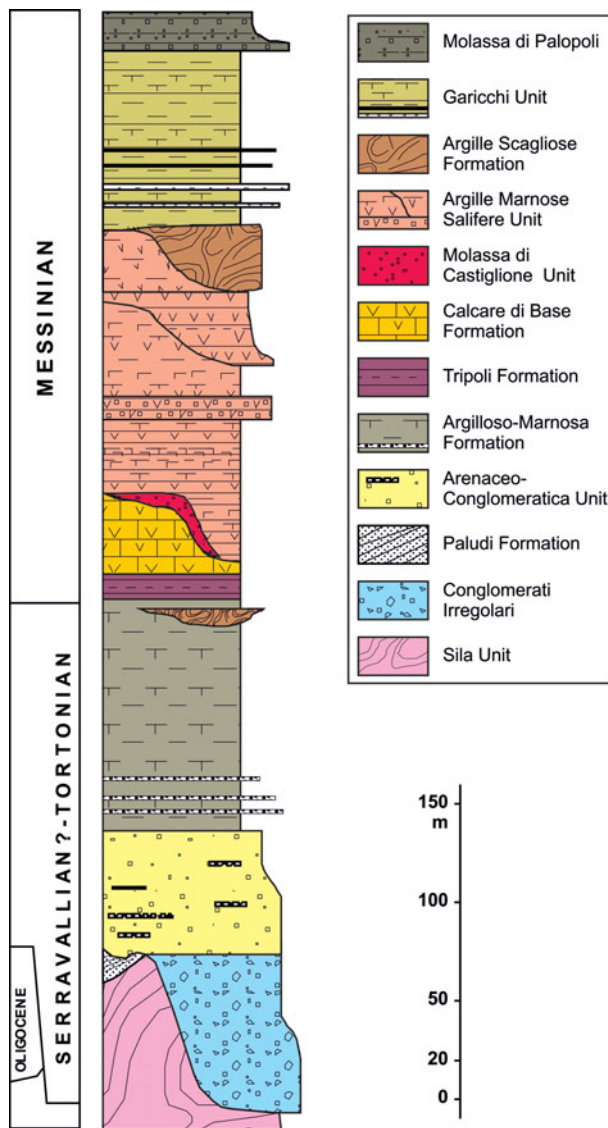
Figure 3. (Colour online) Schematic stratigraphic column of the studied area.

are composed of a variegated clay matrix and olistholiths of various types (calcarenite to calcilutite), marl, chert and quartzose sandstone, equivalent to the typical successions of the Sicilide Complex of the southern Apennines (Critelli & Le Pera, 1998; Critelli, 1999; Zecchin *et al.* 2012).

The transgressive sedimentary fill evolved from cyclic alternations of shale and marl to biosiliceous clay of the Tripoli Formation, which delineates the Tortonian–Messinian boundary. The Tripoli Formation is overlain by the Calcare di Base Formation, which is formed in the studied sector (Figs 2, 3) by a tabular carbonate stratum composed of evaporites and microbial facies, and interbedded with laminar and massive clays and marls (e.g. Barone *et al.* 2008).

The Calcare di Base Formation is overlain, above an erosional angular unconformity, by the Molassa di Castiglione Unit, made up of a basal conglomerate, breccias and cross- to planar stratification sandstones

interpreted as nearshore deposits (e.g. Barone *et al.* 2008).

The Argille Marnose Salifere Unit, consisting of a succession of halite and clayey marls with gypsum-bearing arenites, characterizes the eastern part of the Rossano Basin (Barone *et al.* 2006). These gypsum-bearing arenites are graded and include plane-parallel lamination and ripple intervals; these deposits are interpreted as turbidites. The Argille Marnose Salifere Unit is overlain by large olistostrome bodies having olistoliths and large clasts of Mesozoic and Cenozoic limestone, marl, quartzarenite and chert of the Sicilide Complex terranes of the southern Apennines (e.g. Ogniben, 1955, 1969; Critelli, 1999; Critelli *et al.* 2007, 2011, 2013; Tripodi, Muto & Critelli, 2013).

In the Rossano Basin, the transition from evaporitic to normal marine environments is characterized by the Garicchi Unit (marls and clays with thin turbidite sandstones) and Molassa di Palopoli (conglomerates and sandstones lobes), referred to fluvio-deltaic and deeper-water turbidite systems (e.g. R. Dominici, unpub. Ph.D. thesis, Univ. Calabria, 2005) (Fig. 3).

2.b. Facies associations

In the Rossano Basin the Calcare di Base crops out for about 3 km northeastward of Cropalati (Fig. 2). The unconformity erosionally truncates the limbs of asymmetric folds involving the Calcare di Base, which also underwent previous subaerial exposure, erosion and karstification. As a response to this folding and karstification event, related to both the Messinian Salinity Crisis and to the local regional tectonic phase (i.e. rifting of the southern Tyrrhenian Basin; Patacca, Sartori & Scandone, 1990), a marked increase in sedimentary detritus (Molassa di Castiglione) is detected.

Based on facies and stratigraphic analyses carried out on two sedimentological logs (Fig. 4), we have recognized three facies associations (Fig. 5). The recognition of facies associations in the Calcare di Base in the Rossano Basin represents the first step towards the reconstruction of the sedimentary environment (e.g. R. Dominici, unpub. Ph.D. thesis, Univ. Calabria, 2005).

These two sedimentological logs are characterized by peculiar argillaceous marl beds, which represent important stratigraphic markers (Fig. 4).

2.b.1. Facies A

Facies A consists of decimetre-thick beds of massive limestone made up of micritic, peloidal mudstone or wackestone with minor quartz, feldspar grains and fragments of phyllite and siltstones, interbedded with decimetre-sized vacuolar lenses characterized by gypsum and halite moulds and carbonate pack breccia and float breccia (Fig. 5a, b). The clasts consist of beige and light green, folded or flat pebbles derived from calcilutite.
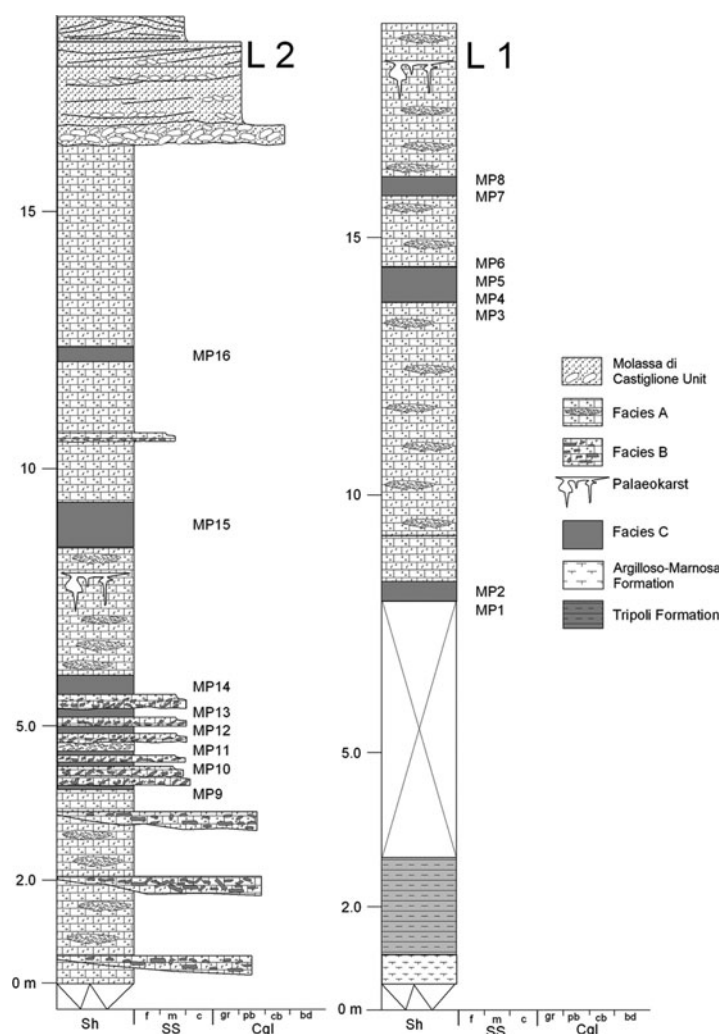
Figure 4. Sedimentological logs of the studied area showing the argillaceous marl samples studied in this work (L1 is the lower part of the stratigraphic succession, whereas L2 is the upper part). Sh – shale; SS – sandstone; Cgl – conglomerate; f – fine; m – medium; c – coarse; gr – gravel; pb –pebble; cb – cobble; bd – boulder.

2.b.2. Facies B

Facies B consists of decimetre-thick, channelled limestone bodies marked by erosional surfaces filled with clay chips, flat pebbles and rip-up clasts within a planar to wavy fine lamination that is generally oriented parallel to layering but sometimes shows oblique laminae (Fig. 5c). Facies B is commonly related to Facies A.

2.b.3. Facies C

Facies C is characterized by decimetre- to centimetre-thick layers of varicoloured, argillaceous marls, which show planar or gently undulating laminae and ripples. Some centimetre-thick rippled layers of graded calcilutite are interbedded with argillaceous marls (Fig. 5d). In some outcrops the contact between Facies C and Facies A and B is associated with cylindrical or conical depressions perpendicular to bedding and filled by breccias, which are interpreted as phreatic conduits and vadose channels (Fig. 5e). Facies A and Facies B pass laterally into a clastic

facies that is also interbedded with Facies C. This clastic facies consists of decimetre- to centimetre-thick calcarenite beds with minor siliciclastic lithic grains and massive to graded breccias containing abundant clay chips, nodular gypsum, minor granite, low-grade metamorphic clasts and rounded sandstone pebbles (Fig. 5f).

Facies A is interpreted as being related to bacterial activity, which induced carbonate precipitation, as suggested by Guido *et al.* (2007). Furthermore the presence of moulds and pseudomorphs of carbonate minerals after evaporite minerals (gypsum and halite) within lenses of carbonate pack breccia and float breccia highlights the growth of evaporitic crystal clusters from groundwater brines in the vadose zone. Facies A is interbedded with Facies B. This can be interpreted as a result of the filling of small tidal channels that dissect intertidal environments.

Facies C records a sharp transition from hypersaline brine (mesohaline–penesaline) to normal saline seawater, probably related to rainfall episodes. In these conditions the sedimentation is driven by erosion processes of the carbonate facies and sedimentary and crystalline
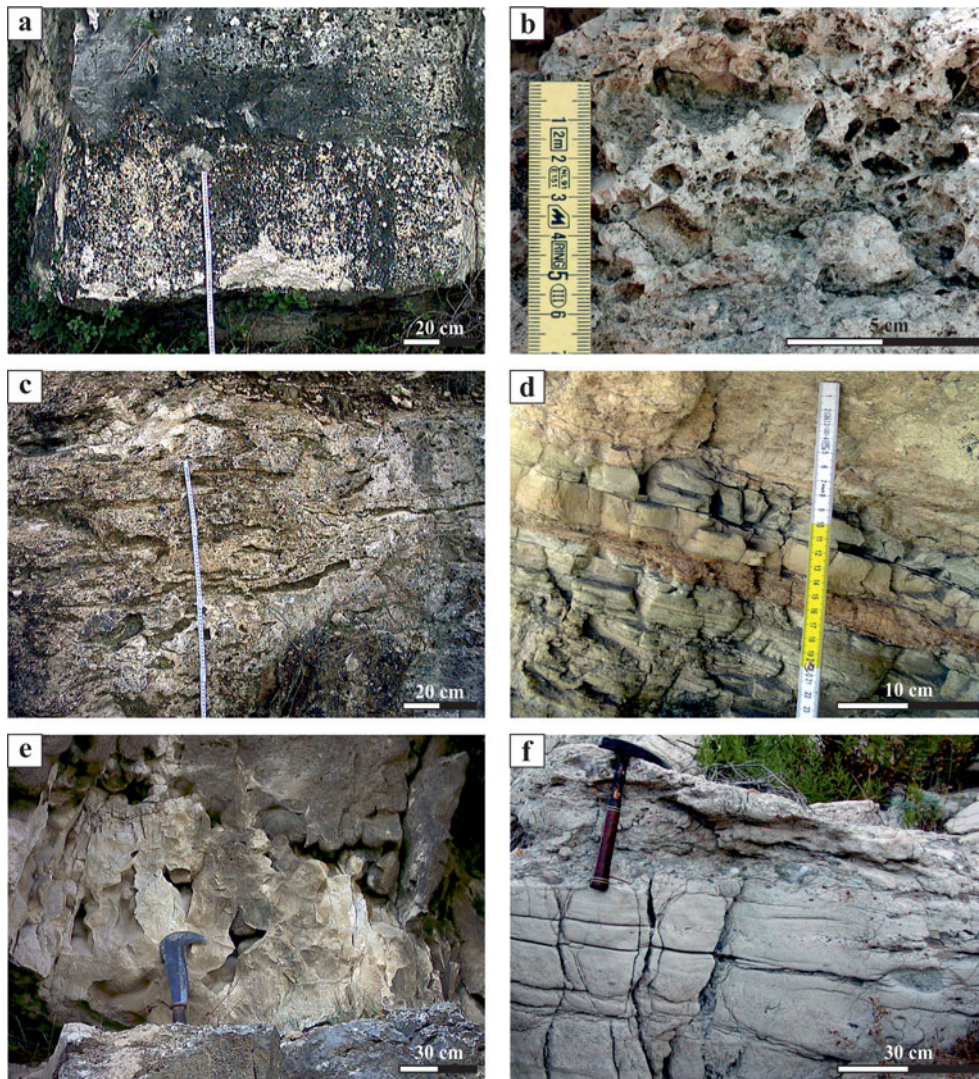
Figure 5. (Colour online) Field photos of the facies associations. (a) Facies A consists of decimetre-thick massive limestone passing upwards to vacuolar mudstone. (b) Close-up view of a pocket characterized by evaporitic pseudomorphs of Facies A. (c) Facies B consists of decimetre-sized clay chips and rip-up clasts of argillaceous marls floating in a micritic matrix. (d) Green and orange argillaceous marls and centimetre-thick layers of graded calcilutite (Facies C). (e) Vadose and phreatic conduits affected the Calcare di Base Formation. (f) Close-up view of clastic facies formed by centimetre-thick graded calcarenites and decimetre-thick limestone gypsum breccias.

units of the continental areas. At the same time, karst processes related to the relative change in sea level affect the Calcare di Base.

The facies observed in the Calcare di Base in the Rossano Basin suggest a shallow marine environment where carbonate precipitation was controlled by bacterial activity followed by diagenesis in the vadose zone by growth and dissolution of evaporite minerals. The association of Facies A, Facies B and Facies C can be interpreted as having been formed in a typical subtidal–intertidal environment. The clastic facies is mainly derived from the erosion of Facies A and Facies B and from Miocene terrigenous units and metamorphic–plutonic rocks of the Sila Unit, formed by gravity deposits located along a gentle ramp (e.g. Critelli & Le Pera, 1998; Le Pera, Critelli & Sorriso-Valvo, 2000; Le Pera *et al.* 2001; R. Dominici, unpub. Ph.D. thesis, Univ. Calabria, 2005).

3. Sampling and methods

A set of 16 argillaceous marl samples from beds interlayered within the Calcare di Base Formation (Fig. 4) were collected along the Rossano Basin (Figs 1, 2).

Samples were cleaned for geochemical analyses. Weathered coats and veined surfaces were cut off. The rocks were crushed and milled in an agate mill to a very fine powder.

The powder was disaggregated in an ultrasonic bath at low power for a few minutes. The mineralogy of the whole-rock powder was obtained by X-ray diffraction (XRD) using a Philips 1710 diffractometer (CuK$_\alpha$ radiation, graphite secondary monochromator, sample spinner; step size 0.02; speed 3 sec for each step) at the Università della Calabria (Italy). Semiquantitative mineralogical analysis of the bulk rock was carried out on random powders measuring peak areas using the WINFIT computer program (Krumm, 1996).

Table 1. Mineralogical composition of the bulk rock (weight per cent)

	Qtz	Σphy	Feld	Dol	Calc	Arag	Gyp	Celest
MP1	16	43	1	4	36	0	0	0
MP2	17	42	1	4	36	0	0	0
MP3	15	38	tr	4	37	3	2	1
MP4	17	37	tr	4	37	3	1	1
MP5	22	47	2	5	22	0	2	tr
MP6	22	48	2	4	22	0	2	tr
MP7	18	38	1	0	37	3	2	1
MP8	15	42	1	0	36	3	2	1
MP9	27	46	2	6	19	0	0	tr
MP10	23	54	2	3	17	0	1	0
MP11	24	53	2	3	17	0	1	0
MP12	23	45	tr	1	28	2	tr	1
MP13	22	46	tr	2	27	2	tr	1
MP14	20	56	2	3	16	1	1	1
MP15	19	57	2	3	16	1	1	1
MP16	23	49	2	4	18	3	0	1

Qtz – quartz; Σphy – sum of phyllosilicates; Feld – feldspars
(K-feldspars + plagioclase); Dol – dolomite; Calc – calcite; Arag –
aragonite; Gyp – gypsum; Celest – celestine; tr – trace.

Elemental analyses for major and some trace element (Nb, Zr, Y, Sr, Rb, Ba, Ni, Co, Cr, V) concentrations were obtained using X-ray fluorescence spectrometry (Philips PW 1480) at the Università della Calabria (Italy), on pressed powder discs of whole-rock samples (prepared by milling to a fine-grained powder in an agate mill) and compared to international standard rock analyses of the United States Geological Survey. X-ray counts were converted into concentrations by a computer program based on the matrix correction method according to Franzini, Leoni & Saitta (1972) and Leoni & Saitta (1976). Total loss on ignition (LOI) was determined by heating the samples for three hours at 900 °C. Instrumental Neutron Activation Analysis (INAA) at the Activation Laboratories (Ancaster, Canada) was used to determine the abundance of the rare earth elements (REEs; La, Ce, Nd, Sm, Eu, Yb and Lu) and Sc, Cs and Th. The estimated precision and accuracy for trace element determinations are better than 5 %, except for those elements having a concentration of 10 ppm or less (10 to 15 %) (e.g. Boström & Bach, 1995; Melaku *et al.* 2004; Mongelli *et al.* 2006; Perri *et al.* 2011; Liu *et al.* 2013).

The chemical composition of sediments (e.g. Th, Sc and REEs) is well suited to provenance and tectonic setting determination studies, because of their relatively low mobility during sedimentary processes (e.g. McLennan, Hemming & Hanson, 1993; Cullers, 2000; Cullers & Podkovyrov, 2002; Mahjoor, Karimi & Rastegarlari, 2009 and references therein). The relative distribution of the immobile elements, which differ in concentration in felsic and basic rocks such as La and Th (enriched in felsic rocks) and Sc, Cr and Co (enriched in basic rocks relative to felsic rocks), has been used to infer the relative contribution of felsic and basic sources in fine-grained sediments from different tectonic environments (e.g. Wronkiewicz & Condie, 1989). The REE pattern of fine-grained siliciclastic sediments and some elemental ratios are assumed to reflect the exposed crustal abundances in the source area

(McLennann, Hemming & Hanson, 1993; Mongelli, Cullers & Muelheisen, 1996; Cullers, 2000; Mongelli, 2004, among others).

4. Mineralogy

The results of the whole-rock XRD analyses are shown in Table 1. The argillaceous marls are mainly composed of phyllosilicates (mostly illite, chlorite, illite/smectite mixed layers and traces of kaolinite) and $CaCO_3$ phases (calcite and aragonite), which prevail over quartz, dolomite and minor/trace amounts of gypsum, feldspars and celestine. Phyllosilicates range from 37 % to 57 % of the total abundances of the minerals. The $CaCO_3$ phases (calcite and aragonite) are the second most abundant minerals, with values ranging from 16 % to 37 % for calcite and up to 3 % for aragonite. Quartz is also abundant (ranging from 15 % to 27 %); dolomite shows values up to 6 %, whereas feldspars (both K-feldspars and plagioclase), gypsum and celestine are minor or present in trace amounts in many samples (Table 1).

5. Whole-rock geochemistry

To better examine the geochemical features of the studied samples, the argillaceous marl compositions are normalized to standard clay-rich lithologies of the PAAS (Post-Archaean Australian Shale; Taylor & McLennan, 1985) (Fig. 6). The elemental concentrations and the ratios are given in Table 2; means, standard deviations and ranges of values for the elemental contents and some ratios are given in Table 3.

Ca and Sr share the same distribution over the entire studied succession, matching the abundance of the $CaCO_3$ phases, such as calcite and aragonite. Sr, however, is strongly enriched relative to the PAAS, rather than Ca, since its distribution is also related to celestine, occurring in many samples as a minor or trace phase. Mg is enriched relative to the PAAS due to the

Table 2. Distribution of major and trace elements and ratios in the studied samples

Samples	MP1	MP2	MP3	MP4	MP5	MP6	MP7	MP8
Oxides (wt %)								
SiO_2	29.70	29.52	28.49	28.60	37.58	37.15	27.44	26.98
TiO_2	0.32	0.28	0.31	0.34	0.36	0.32	0.30	0.29
Al_2O_3	7.17	6.98	6.84	6.52	8.32	8.29	6.65	7.10
Fe_2O_3	6.31	6.10	6.37	6.15	5.19	5.16	6.11	6.49
MnO	0.22	0.21	0.22	0.18	0.12	0.14	0.21	0.19
MgO	3.32	3.28	6.19	6.05	6.83	6.74	6.00	5.92
CaO	22.61	22.42	25.42	25.11	15.36	15.21	24.46	23.98
Na_2O	0.40	0.42	0.53	0.49	0.52	0.50	0.41	0.42
K_2O	1.14	1.19	1.09	1.07	1.43	1.39	1.04	1.06
P_2O_5	0.11	0.10	0.07	0.10	0.17	0.18	0.07	0.07
LOI	28.65	28.84	24.41	24.60	24.13	24.86	27.20	26.87
TOT	99.95	99.34	99.94	99.21	100.01	99.94	99.89	99.37
Trace elements (ppm)								
Ni	77.00	71.00	70.00	68.00	66.00	67.00	71.00	74.00
Cr	84.00	80.00	75.00	71.00	93.00	96.00	72.00	75.00
Co	20.00	18.00	16.00	17.00	20.00	21.00	17.00	19.00
V	117.00	108.00	90.00	95.00	121.00	119.00	97.00	100.00
Sc	8.50	8.00	8.40	8.00	8.50	8.20	7.10	7.20
Ba	148.00	152.00	208.00	200.00	209.00	201.00	197.00	200.00
Cs	7.80	7.10	7.10	7.50	6.20	6.50	6.00	7.00
Sr	1921.00	1915.00	13178.00	13250.00	5082.00	5074.00	13256.00	13195.00
Rb	87.00	81.00	70.00	78.00	101.00	99.00	73.00	75.00
Nb	6.00	5.00	1.00	2.00	8.00	7.20	1.00	1.00
Zr	167.00	180.00	566.00	540.00	261.00	259.00	573.00	569.00
Y	1.00	2.00	1.00	1.00	13.00	9.00	3.00	4.00
Th	5.60	5.50	6.00	5.70	5.60	5.50	5.10	5.20
La	21.50	21.10	21.40	21.20	19.90	20.10	20.60	20.50
Ce	33.00	31.00	35.00	34.00	30.00	32.00	34.00	32.00
Nd	14.00	15.00	13.00	14.00	15.00	16.00	15.00	14.00
Sm	3.60	3.80	3.70	3.60	3.30	3.50	3.40	3.50
Eu	0.80	0.70	0.80	0.90	0.70	0.80	0.70	0.82
Yb	1.60	1.50	1.70	1.80	1.40	1.50	1.30	1.40
Lu	0.24	0.23	0.25	0.26	0.21	0.22	0.20	0.21
Ratios								
CIA	66.18	66.16	65.06	64.38	66.78	67.66	66.62	67.23
CIA′	75.36	74.02	73.65	73.42	73.72	74.25	75.13	75.96
La/Sc	2.53	2.64	2.55	2.65	2.34	2.45	2.90	2.85
Th/Sc	0.66	0.69	0.71	0.71	0.66	0.67	0.72	0.72
Th/Co	0.28	0.31	0.38	0.34	0.28	0.26	0.30	0.27
Th/Cr	0.07	0.07	0.08	0.08	0.06	0.06	0.07	0.07
Cr/Th	15.00	14.55	12.50	12.46	16.61	17.45	14.12	14.42

Samples	MP9	MP10	MP11	MP12	MP13	MP14	MP15	MP16
Oxides (wt %)								
SiO_2	39.91	38.06	37.98	36.65	37.02	37.59	37.65	38.91
TiO_2	0.33	0.47	0.46	0.37	0.38	0.45	0.44	0.39
Al_2O_3	7.93	10.69	10.52	8.26	8.89	10.80	10.95	8.96
Fe_2O_3	3.95	11.17	11.02	6.60	6.82	11.54	11.61	8.11
MnO	0.11	0.12	0.14	0.20	0.19	0.12	0.13	0.25
MgO	7.13	4.38	4.45	3.78	3.82	3.94	4.01	5.97
CaO	13.62	11.45	11.12	17.54	17.63	11.22	11.11	13.39
Na_2O	0.36	0.46	0.45	0.36	0.37	0.39	0.42	0.38
K_2O	1.33	1.70	1.69	1.37	1.40	1.70	1.68	1.49
P_2O_5	0.11	0.08	0.10	0.12	0.11	0.09	0.10	0.08
LOI	25.21	21.34	21.95	24.12	23.11	22.05	21.65	22.01
TOT	99.99	99.92	99.88	99.37	99.74	99.89	99.75	99.94
Trace elements (ppm)								
Ni	62.00	102.00	95.00	56.00	57.00	101.00	91.00	84.00
Cr	88.00	119.00	121.00	93.00	101.00	135.00	131.00	102.00
Co	18.00	32.00	33.00	20.00	23.00	35.00	34.00	25.00
V	119.00	165.00	159.00	117.00	121.00	190.00	189.00	143.00
Sc	8.50	9.50	9.60	8.00	8.20	10.20	10.10	9.20
Ba	202.00	193.00	195.00	268.00	259.00	208.00	211.00	195.00
Cs	6.90	11.50	10.90	6.60	7.10	11.70	11.10	8.10
Sr	4440.00	1742.00	1719.00	12396.00	12289.00	10447.00	10339.00	14881.00
Rb	104.00	120.00	118.00	86.00	91.00	111.00	115.00	93.00
Nb	3.00	11.00	10.00	4.00	6.00	8.00	9.00	4.00
Zr	218.00	132.00	143.00	568.00	559.00	474.00	481.00	673.00
Y	1.00	2.00	3.00	5.00	3.00	2.00	4.00	11.00
Th	5.90	5.70	5.80	5.50	5.60	6.30	6.10	6.20
La	20.40	23.30	23.50	19.80	20.10	26.40	25.90	24.80
Ce	33.00	34.00	35.00	30.00	32.00	39.00	37.00	38.00
Nd	16.00	15.00	17.00	15.00	16.00	22.00	21.00	19.00

Table 2. Continued.

Samples	MP1	MP2	MP3	MP4	MP5	MP6	MP7	MP8
Sm	3.50	3.70	3.80	3.20	3.30	4.10	4.20	4.30
Eu	0.70	0.90	1.00	0.70	0.80	1.00	0.90	0.90
Yb	1.50	1.60	1.70	1.40	1.40	1.50	1.60	1.60
Lu	0.23	0.24	0.23	0.21	0.22	0.23	0.24	0.24
Ratios								
CIA	67.42	71.88	73.45	72.63	71.50	72.05	72.84	72.97
CIA′	75.41	76.39	76.26	75.72	76.64	77.11	77.29	75.78
La/Sc	2.40	2.45	2.45	2.48	2.45	2.59	2.56	2.70
Th/Sc	0.69	0.60	0.60	0.69	0.68	0.62	0.60	0.67
Th/Co	0.33	0.18	0.18	0.28	0.24	0.18	0.18	0.25
Th/Cr	0.07	0.05	0.05	0.06	0.06	0.05	0.05	0.06
Cr/Th	14.92	20.88	20.86	16.91	18.04	21.43	21.48	16.45

Table 3. Means, standard deviations and ranges of elemental concentrations and ratios of the studied samples

	Mean	St. Dev.	Min.	Max.
Oxides (wt. %)				
SiO$_2$	34.33	4.64	26.98	39.91
TiO$_2$	0.36	0.06	0.28	0.47
Al$_2$O$_3$	8.43	1.52	6.52	10.95
Fe$_2$O$_3$	7.42	2.42	3.95	11.61
MnO	0.17	0.04	0.11	0.25
MgO	5.11	1.31	3.28	7.13
CaO	17.60	5.37	11.11	25.42
Na$_2$O	0.43	0.05	0.36	0.53
K$_2$O	1.36	0.24	1.04	1.70
P$_2$O$_5$	0.10	0.03	0.07	0.18
LOI	24.44	2.35	21.34	28.84
Trace elements (ppm)				
Ni	75.75	14.24	56.00	102.00
Cr	96.00	20.20	71.00	135.00
Co	23.00	6.46	16.00	35.00
V	128.13	30.92	90.00	190.00
Sc	8.58	0.89	7.10	10.20
Ba	202.88	28.97	148.00	268.00
Cs	8.07	1.94	6.00	11.70
Sr	8445.25	4903.36	1719.00	14881.00
Rb	93.88	15.97	70.00	120.00
Nb	5.39	3.19	1.00	11.00
Zr	397.69	186.84	132.00	673.00
Y	4.06	3.60	1.00	13.00
Th	5.71	0.32	5.10	6.30
La	21.91	2.11	19.80	26.40
Ce	33.69	2.57	30.00	39.00
Nd	16.06	2.46	13.00	22.00
Sm	3.66	0.31	3.20	4.30
Eu	0.82	0.10	0.70	1.00
Yb	1.53	0.13	1.30	1.80
Lu	0.23	0.02	0.20	0.26
Ratios				
CIA	69.05	3.14	64.38	73.45
CIA′	75.38	1.21	73.42	77.29
La/Sc	2.56	0.15	2.34	2.90
Th/Sc	0.67	0.04	0.60	0.72
Th/Co	0.26	0.06	0.18	0.38
Th/Cr	0.06	0.01	0.05	0.08
Cr/Th	16.75	2.96	12.46	21.48
(La/Yb)ch	9.70	0.96	7.96	11.89
Ce/Ce*	0.74	0.04	0.68	0.81

St. Dev. – standard deviation; Min. – minimum value; Max. – maximum value.

abundance of dolomite (Table 1). Furthermore, a weak correlation between Mg and Si, Al and Fe suggests that clay minerals played a minor role in hosting Mg, indicating that Mg fluctuations are influenced mainly by the distribution of dolomite.

The Si, Ti, Al, Na, K and P concentrations have a similar distribution throughout the succession, and are generally depleted relative to values for the PAAS. The degree of depletion of Na, K and Al is probably related to the paucity of feldspars (Fig. 6). Nb, having a
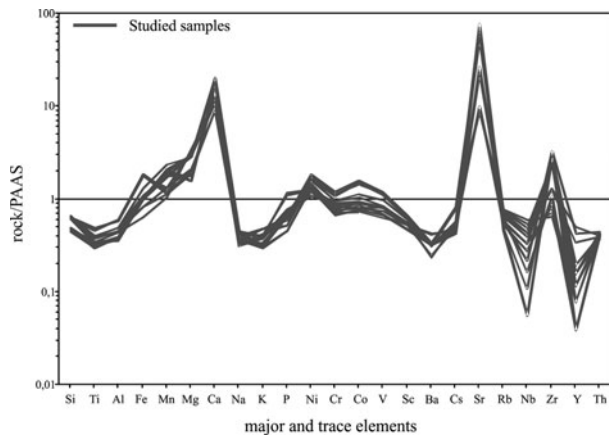
Figure 6. Major and trace element compositional ranges normalized to the PAAS (Post-Archaean Australian Shale; Taylor & McLennan, 1985).
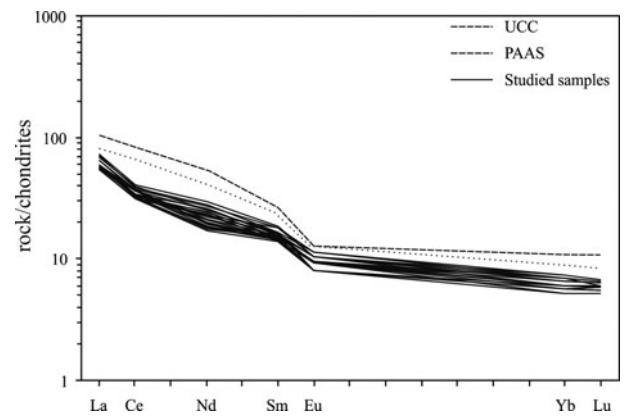

Figure 7. Rare earth element compositional ranges, chondrite-normalized (Taylor & McLennan, 1985). The plot of the Post-Archaean Australian Shale (PAAS) and the Upper Continental Crust (UCC; McLennan, Taylor & Hemming, 2006) is shown for comparison.

similar geochemical behaviour to that of Ti, is strongly depleted in concentration relative to that in the PAAS (Fig. 6).

Fe, Mn and the TEs (transition trace elements; e.g. Sc, V, Cr, Co and Ni) yield a trend similar as those in the PAAS, with some samples showing a weak enrichment relative to the PAAS (Fig. 6). Fe, showing a positive correlation with all TEs, is hosted by mica-like clay minerals; thus, the supply of these elements, having the same mineralogical controls on their distribution, is mainly related to the presence of clay minerals.

The distributions of HFSEs (high-field-strength elements; e.g. REEs, Zr, Th and Y) are different; Th and Y concentrations, similarly to Nb, are strongly depleted relative to those in the PAAS, whereas Zr is enriched in many samples (Fig. 6). Most investigations have reported rather low concentrations of REEs in sedimentary carbonate rocks (e.g. Taylor & McLennan, 1985). In marine carbonates, a distinct Ce depletion is common, reflecting the Ce depletion in seawater relative to the other REEs (Taylor & McLennan, 1985). The studied samples show low total REE contents (average $\Sigma REE = 77.89 \pm 7.30$); both light rare earth elements (LREEs) and heavy rare earth elements (HREEs) are depleted relative to the PAAS and Upper Continental Crust (UCC) values (Fig. 7). Generally, the chondrite-normalized REE patterns (Fig. 7) show a marked LREE to HREE fractionation (values of (La/Yb)ch ranging from 7.96 to 11.89, with many samples characterized by (La/Yb)ch values higher than those of the PAAS and UCC and a mean of (La/Yb)ch = 9.70 ± 0.96; Table 3) compared to the PAAS (9.17) and UCC (9.21), and a negative Ce anomaly (Ce/Ce* = 0.74 ± 0.04) typical of a seawater environment.

The LILEs (large ion lithophile trace elements; e.g. Rb, Cs and Ba) are associated in sediments with the detrital minerals (e.g. Plank & Langmuir, 1998). The Rb, Cs and Ba concentrations, similar to K, are depleted relative to those in the PAAS (Fig. 6). In the present case, the 'lack' of feldspar means that Rb, Cs and K

are likely hosted by the 2:1 clay minerals as revealed by XRD analysis.

6. Discussion

6.a. Palaeoweathering, palaeoclimate and depositional environment

Various indices have been used to reconstruct palaeoweathering conditions, including the chemical index of alteration (CIA; Nesbitt & Young, 1982), the chemical index of weathering (CIW; Harnois, 1988), the plagioclase index of alteration (PIA; Fedo, Nesbitt & Young, 1995) and the weathering index (Ohta & Arai, 2007). The CIA is expressed as the molar volumes of $(Al/(Al + Ca^* + Na + K)) \times 100$, where Ca^* represents the CaO only from the silicate fraction (Nesbitt & Young, 1982). As the samples contain some carbonate, the CPA (chemical proxy of alteration) after Buggle *et al.* (2011) (or CIW, chemical index of weathering after Cullers, 2000) is often additionally used. In this study, both the CIA (Nesbitt & Young, 1982; with the CaO values of the silicate fraction only) and the CIA′ (the molar volumes of $(Al/(Al + Na + K)) \times 100$ and, thus, calculated without the CaO content) have been used.

The argillaceous marls have CIA values (average CIA = 69.05 ± 3.14) typical of moderate palaeoweathering conditions. The A–CN–K plot (Fig. 8a) of the samples show a weathering trend parallel to the A–CN edge, departing from a granitic source towards the shale composition and indicating non-steady-state weathering conditions. Tectonism and climate generally determine the relative rates of erosion and chemical weathering (Taylor & McLennan, 1985; McLennan, Hemming & Hanson, 1993). The pattern in the A–CN–K plot (Fig. 8a) is typical of a source area in which active tectonism allows erosion of all zones within weathering profiles developed on source rocks (Nesbitt, Fedo & Young, 1997). Furthermore, the samples are characterized by a weathering trend (Fig. 8b) and CIA′
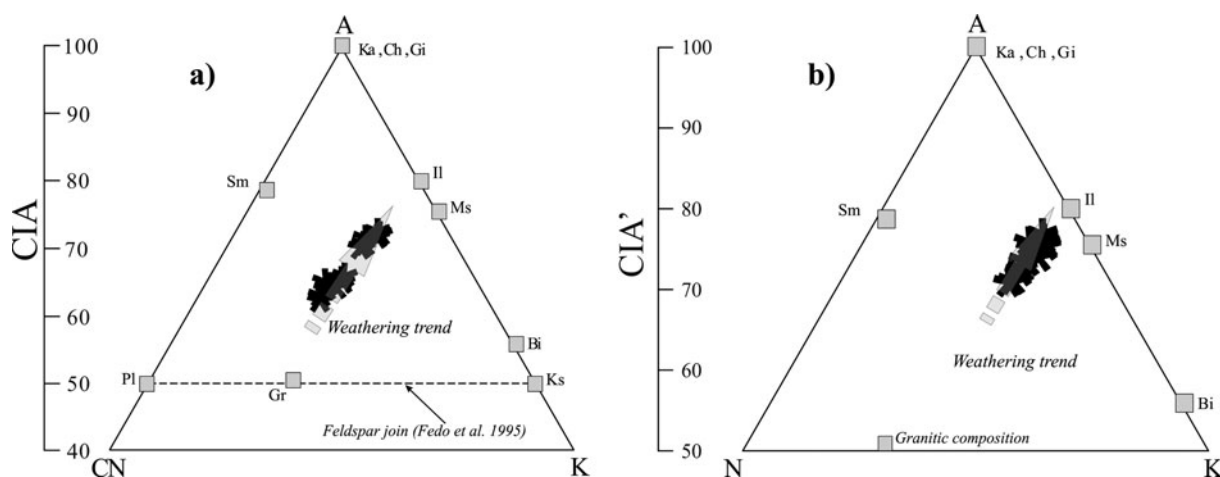
Figure 8. (a) Ternary A–CN–K and (b) A–N–K diagrams. Legend: Gr – granite; Ms – muscovite; Il – illite; Ka – kaolinite; Ch – chlorite; Gi – gibbsite; Sm – smectite; Bi – biotite; Pl – plagioclase; Ks – K-feldspar; A – Al_2O_3; CN – $CaO+Na_2O$; K – K_2O; CIA – Chemical Index of Alteration (Nesbitt & Young, 1982).

(average CIA$'$ = 75.38 ± 1.21) similar to CIA values, also testifying to moderate palaeoweathering conditions.

As a broad measure of weathering, it is possible to use certain molecular ratios. The Rb/K ratio has been used to monitor palaeoweathering because both K and Rb are incorporated into clay minerals and because K is preferentially leached over Rb with increased intensity of weathering (e.g. Wronkiewicz & Condie, 1989; Peltola *et al.* 2008).

Very low values of Rb/K (< 0.01) are found for the argillaceous marls, indicating weak to moderate weathering in a dry climate (e.g. Mongelli *et al.* 2012), which is also indicated by the mineralogical composition. The moderate weathering may have occurred under slightly warmer conditions than those of the present, as reported by Matson & Fox (2010) for SE Spain. Slight variations of K/Rb ratios suggest that persistent, dry and warm conditions changed to conditions characterized by alternating dry and relatively wet periods, typical of the climatic cycle in savannah regions (e.g. Mongelli *et al.* 2012).

The argillaceous marls are characterized by higher variations in Sr compared to the other trace elements. In sedimentary processes, the distribution of Sr is affected both by strong adsorption on clay minerals and extensive substitution of Sr^{2+} for Ca^{2+} in carbonate minerals (aragonite > calcite) (e.g. Salminen *et al.* 2005). High Sr/Ca ratios in carbonate sediments are inferred to correspond to aragonite enrichment (Thomson *et al.* 2004). The Sr distribution is generally controlled by the preferential incorporation into the Ca sites, such as in the aragonite structure in which Sr and Ca show a good correlation. In the present case, Sr is weakly correlated with Ca, testifying to a main link to celestine precipitation and adsorption on clay minerals, as shown by XRD analyses (Table 1). Furthermore, higher Sr concentrations are typical of marine to hypersaline environments (e.g. Land, 1980), whereas lower Sr concentrations characterize ancient

marine or marine–meteoric environments (Machel & Anderson, 1989). The incorporation of Sr^{2+} into aragonite appears to be independent of salinity (Gaetani & Cohen, 2006). Sr variations, ranging from 1719 ppm to 14 881 ppm (Table 2), suggest a transition from depositional environments, characterized by normal marine waters and normal evaporation, to hypersaline environments with strong evaporation. As a whole, these data seem to reflect that deposition probably occurred in a semi-closed marine environment subject to hypersalinity with local periodic input of meteoric water (e.g. Guido *et al.* 2007).

6.b. Parental affinity, sorting and recycling

REEs and Th, among the HFSEs, and some transition elements, including Sc, V and Ni, can constrain the average source area composition (e.g. Taylor & McLennan, 1985; McLennan, Hemming & Hanson, 1993; Cullers & Podkovyrov, 2002). The abundance of Cr and Ni in clastic sediments is considered a useful indicator in provenance studies. According to Wrafter & Graham (1989) a low concentration of Cr indicates a felsic provenance, whereas high contents of Cr and Ni are mainly found in sediments derived from ultramafic rocks (Armstrong-Altrin *et al.* 2004). The Cr/Ni ratios are low for the argillaceous marls (average = 1.28). Furthermore, the Th/Cr ratios (average = 0.06) are lower than those of the PAAS (Th/Cr = 0.13; Taylor & McLennan, 1985) and the UCC (Th/Cr = 0.13; McLennan, Taylor & Hemming, 2006). The La/Sc, Th/Sc, Th/Co, Th/Cr and Cr/Th ratios are significantly different in felsic and basic rocks and may also allow constraints on the average provenance composition (Wronkiewicz & Condie, 1989; Cox, Lowe & Cullers, 1995). These elemental ratios of argillaceous marls are compared with those of sediments derived from felsic and basic rocks as well as to the UCC (McLennan, Taylor & Hemming, 2006) and the PAAS (Taylor & McLennan, 1985) values (Table 4). The

Table 4. Range of elemental ratios of studied samples compared to the ratios those of felsic and mafic rocks, Upper Continental Crust (UCC) and Post-Archaean Australian Shale (PAAS)

| Elemental ratio | Average values of argillaceous marls | Range of sediments[1] | | Upper Continental Crust[2] | Post-Archaean Australian average shale[3] |
		Felsic rocks	Mafic rocks		
La/Sc	2.60	2.5–16.3	0.4–0.8	2.21	2.40
Th/Sc	0.70	0.8–20.5	0.1–0.2	0.79	0.90
Th/Co	1.00	0.6–19.4	0.1–1.4	0.63	0.64
Th/Cr	0.10	0.1–2.7	0.4–0.8	0.13	0.13
Cr/Th	7.21	4.0–15.0	25–500	7.69	7.53

[1]Cullers (1994, 2000); Cullers & Podkovyrov (2002); [2]McLennan, Taylor & Hemming (2006); [3]Taylor & McLennan (1985).
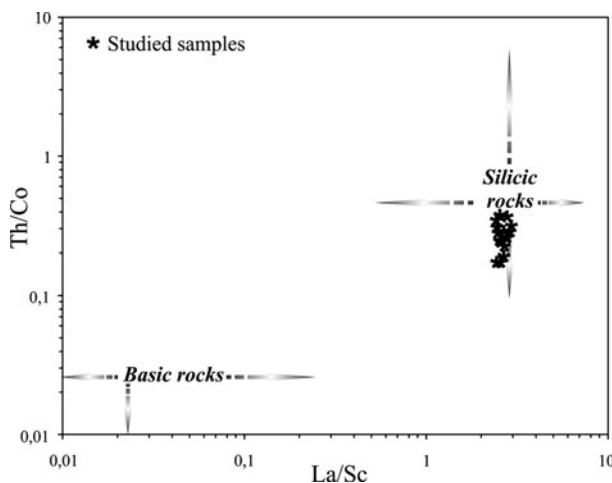
Figure 9. Th/Co versus La/Sc diagram for argillaceous marls (fields after Cullers, 2002).
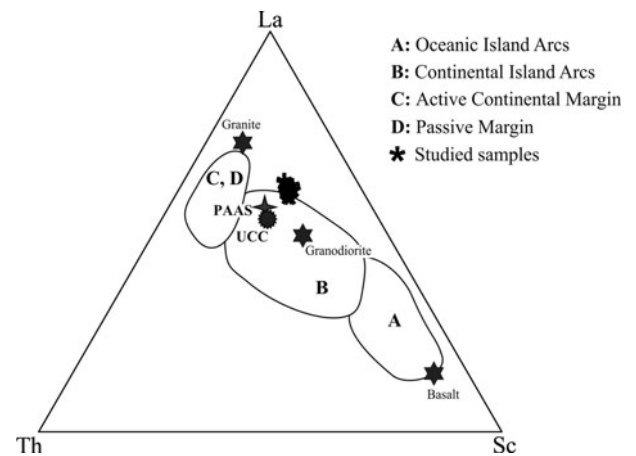

Figure 10. La–Th–Sc diagram (after Bhatia & Crook, 1986). The studied samples fall in a region close to the PAAS and the UCC point that rules out important mafic supply.
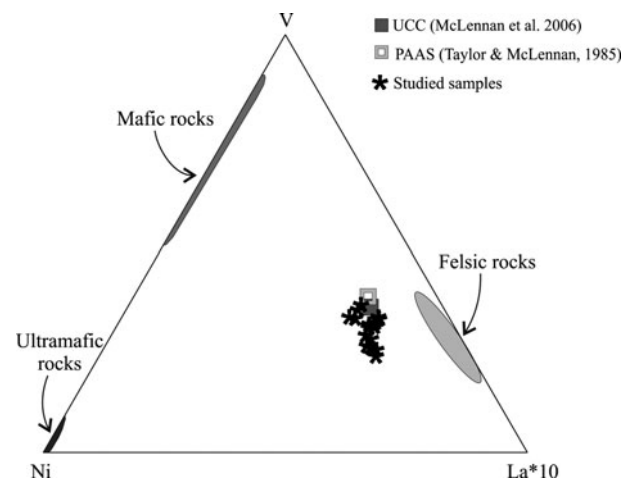

Figure 11. V–Ni–La*10 ternary diagram, showing fields representative of felsic, mafic and ultramafic rocks plot separately (e.g. Bracciali *et al.* 2007; Perri, Muto & Belviso, 2011). The studied samples plot close to the felsic composition and to the Palaeozoic basement rocks analysed in this work.

average values of the argillaceous marls fall within the range of felsic rocks. In addition, the average values of the studied samples are close to those of the PAAS and UCC (Table 4), suggesting a felsic nature of the source rocks. Felsic igneous rocks are generally enriched in Zr relative to mafic lithologies (e.g. Salminen *et al.* 2005). Many argillaceous marls show Zr enrichment relative to the PAAS. Thus, elevated total Zr values are indicative of provenance from felsic rocks, especially intrusive granitoids (e.g. Salminen *et al.* 2005) such as the Sila Batholith. The Th/Co versus La/Sc plot may be used to discriminate sediments from silicic sources from those from progressively more basic sources (Fig. 9). The argillaceous marls fall within the silicic rock field. Furthermore, the La–Th–Sc diagram (Fig. 10) may be used to discriminate the source area composition and the tectonic setting (e.g. Bhatia & Crook, 1986; Cullers, 1994). In this diagram, the argillaceous marls fall in a region close to the PAAS and the UCC, again suggesting a mostly silicic provenance (Fig. 10). To better constrain the felsic versus mafic or ultramafic character of the detritus, the V–Ni–La*4 ternary diagram (Fig. 11) has been used with fields representative of felsic, mafic and ultramafic rocks (e.g. Bracciali *et al.* 2007; Perri, Muto & Belviso, 2011). As a general rule, the studied samples plot close to the

UCC and PAAS area, reflecting the felsic composition of the source areas (Fig. 11).

Transport and deposition of clastic sediments involve mechanical sorting affecting the chemical composition of terrigeneous sediments and the distribution of provenance and palaeoweathering proxies (Perri *et al.*
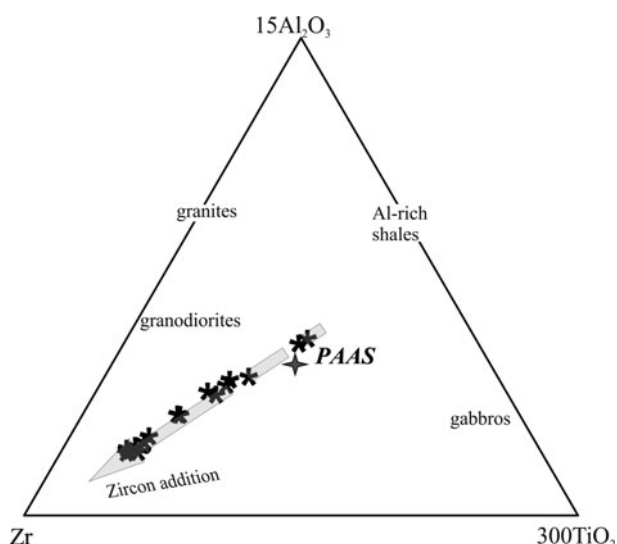
Figure 12. Ternary $15Al_2O_3$–$300TiO_2$–Zr plot (Garcia, Coehlo & Perrin, 1991) showing possible sorting effects for the studied samples.
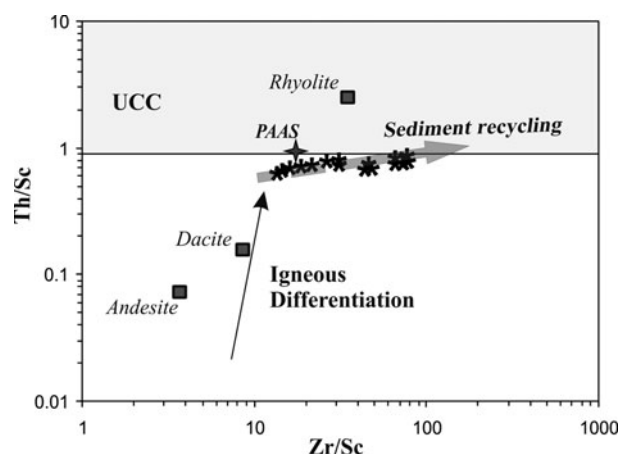

Figure 13. Th/Sc versus Zr/Sc plot (after McLennan, Hemming & Hanson, 1993). Samples depart from the compositional trend indicating zircon addition suggestive of a recycling effect. Rock average compositions (Rhyolite, Dacite and Andesite) are from Lacassie, Hervè & Roser (2006).

2013 and references therein). The distribution of the chemical components within a suite is mainly determined by the mechanical properties of the host minerals. The process basically fractionates Al (clay minerals) from Si (quartz and feldspars). Sorting also fractionates Ti, which is mostly present in clay minerals and Ti oxides, from Zr, which occurs in zircon and is sorted with quartz. Ternary plots based on Al, Ti and Zr may used to illustrate the presence of sorting-related fractionations, which are recognized by simple mixing trends on a ternary Al–Ti–Zr diagram (Garcia, Coehlo & Perrin, 1991). The argillaceous marls show a mixing trend, mostly characterized by changes in the Al/Zr ratio, which could be due to a recycling effect (Fig. 12). The presence of sorting-related fractionations may also be evaluated when the Zr/Sc ratio (Cox, Lowe & Cullers, 1995) is plotted against the Th/Sc ratio (indicator of chemical differentiation; McLennan, Hemming & Hanson, 1993). The studied samples are not clustered along the primary compositional trend but fall along a trend involving zircon addition and thus sediment recycling (Fig. 13), consistent with the Al–Ti–Zr diagram.

7. Concluding remarks

During late Miocene time, Calabria was affected by climatic and environmental changes that involved the entire Mediterranean Basin following the Messinian Salinity Crisis. The Messinian argillaceous marls, interbedded within the Calcare di Base Formation in the Rossano Basin, provide new insight into one of the most intensively studied evaporitic events of the Earth's history. These deposits comprise an admixture of clay minerals, carbonates and quartz with a minor amount of gypsum, feldspars and celestine. The analysed samples show some geochemical and mineralogical differences, reflecting changes in climatic and environmental con-

ditions. Messinian argillaceous marls record deposition that probably occurred in a semi-closed marine environment mainly subject to hypersalinity with local episodes of meteoric water influx, during a period characterized by persistent dry and warm/arid conditions alternating with relatively wet phases, typical of the climatic cycle in savannah regions. The presence of celestine indicates concentration of SO_4^{2-} in the solution from which dolomite formed, as also observed in many modern hypersaline environments (e.g. Corzo *et al.* 2005; Last & Ginn, 2005). Bacterial degradation of organic matter produced CO_2 and ammonia, thereby increasing alkalinity, which may further explain the formation of dolomite under hypersaline conditions (Sánchez-Román *et al.* 2009).

The geochemical proxies indicate a felsic composition for the source area(s), mainly characterized by the Sila Unit and granitoids of the Sila Batholith. The weathering indices indicate moderate palaeoweathering conditions related to a source area where active tectonism allows erosion of all zones within weathering profiles developed on source rocks. Furthermore, the presence of sorting-related fractionations and, thus, sediment recycling is also evaluated using the Th/Sc versus Zr/Sc plot and the Al–Ti–Zr diagram.

References

ALGEO, T. J. & MAYNARD, J. B. 2004. Trace-element behavior and redox facies in core shales of Upper Pennsylvanian Kansastype cyclothems. *Chemical Geology* **206**, 289–318.

ARMSTRONG-ALTRIN, J. S., LEE, Y., VERMA, S. & RAMASAMY, S. 2004. Geochemistry of sandstones from the upper Miocene Kudankulam Formation, southern India: implications for provenance, weathering, and tectonic setting. *Journal of Sedimentary Research* **74**, 285–97.

BARONE, M., CRITELLI, S., LE PERA, E., DI NOCERA, S., MATANO, F. & TORRE, M. 2006. Stratigraphy and detrital modes of Upper Messinian post-evaporitic sandstones of the Southern Apennines, Italy: evidence of foreland-basin evolution during the Messinian Mediterranean salinity crisis. *International Geology Review* **48**, 702–24.

BARONE, M., DOMINICI, R., MUTO, F. & CRITELLI, S. 2008. Detrital modes in a late Miocene wedge-top basin, northeastern Calabria, Italy: compositional record of wedge-top partitioning. *Journal of Sedimentary Research* **78**, 693–711.

BHATIA, M. R. & CROOK, K. A. W. 1986. Trace element characteristics of graywackes and tectonic setting discrimination of sedimentary basins. *Contribution to Mineralogy and Petrology* **92**, 181–93.

BONARDI, G., CAVAZZA, W., PERRONE, V. & ROSSI, S. 2001. Calabria-Peloritani Terrane and Northern Ionian Sea. In *Anatomy of an Orogen: The Apennines and Adjacent Mediterranean Basins* (eds G. B. Vai & I. P. Martini), pp. 287–306. Dordrecht/Boston/London: Kluwer Academic Publishers.

BONARDI, G., DE CAPOA, P., DI STASO, A., PERRONE, V., SONNINO, M. & TRAMONTANA, M. 2005. The age of the Paludi Formation: a major constraint to the beginning of the Apulia-verging orogenic transport in the northern sector of the Calabria-Peloritani Arc. *Terra Nova* **17**, 331–37.

BOSTRÖM, K. & BACH, W. 1995. Trace element determinations by X-ray fluorescence analysis: advantages, limitations, and alternatives. In *Proceedings of the Ocean Drilling Program, Scientific Results, vol. 142* (eds R. Batiza, M. A. Storms & J. F. Allan), pp. 61–8. College Station, Texas.

BRACCIALI, L., MARRONI, M., LUCA, P. & SERGIO, R. 2007. Geochemistry and petrography of Western Tethys Cretaceous sedimentary covers (Corsica and Northern Apennines): from source areas to configuration of margins. *Geological Society of America Special Papers* **420**, 73–93.

BUGGLE, B., GLASER, B., HAMBACH, U., GERASIMENKO, N. & MARKOVIĆ, S. 2011. An evaluation of geochemical weather indices in loess-paleosol studies. *Quaternary International* **240**, 12–21.

CARACCIOLO, L., GRAMIGNA, P., CRITELLI, S., CALZONA, A. B. & RUSSO, F. 2013. Petrostratigraphic analysis of a Late Miocene mixed siliciclastic-carbonate depositional system (Calabria, Southern Italy): implications for Mediterranean paleogeography. *Sedimentary Geology* **284**, 117–32.

CARACCIOLO, L., LE PERA, E., MUTO, F. & PERRI, F. 2011. Sandstone petrology and mudstone geochemistry of the Peruc-Korycany Formation (Bohemian Cretaceous Basin, Czech Republic). *International Geology Review* **53**, 1003–31.

CIANFLONE, G. & DOMINICI, R. 2011. Physical stratigraphy of the upper Miocene sedimentary succession in the northeastern Catanzaro Through (Central Calabria, Italy). *Rendiconti Online della Società Geologica Italiana* **17**, 63–9.

CIANFLONE, G., DOMINICI, R. & SONNINO, M. 2012. Preliminary study of the primary and resedimented Messinian facies of the Northeastern sector of Catanzaro Trough. *Rendiconti Online della Società Geologica Italiana* **21**, 71–3.

CIESM. 2008. The *Messinian Salinity Crisis from Mega-Deposits to Microbiology – A Consensus Report. Almeria, Spain, 7–10 November 2007.* CIESM Workshop Monographs no. 33, pp. 1–28. Monaco: CIESM.

CORZO, A., LUZON, A., MAYAYO, M., VAN BERGEIJK, S., MATA, P. & GARCIA DE LOMAS, L. 2005. Carbonate mineralogy along a biogeochemical gradient in recent lacustrine sediments of Gallocanta Lake (Spain). *Geomicrobiology Journal* **22**, 283–98.

COX, R., LOWE, D. & CULLERS, R. L. 1995. The influence of sediment recycling and basement composition on evolution of mudrock chemistry in southwestern United States. *Geochimichima et Cosmochimica Acta* **59**, 2919–40.

CRITELLI, S. 1999. The interplay of lithospheric flexure and thrust accommodation in forming stratigraphic sequences in the southern Apennines foreland basin system, Italy. *Memorie dell'Accademia Nazionale dei Lincei* **10**, 257–326.

CRITELLI, S. & LE PERA, E. 1995. Tectonic evolution of the Southern Apennines thrust-belt (Italy) as reflected in modal compositions of Cenozoic sandstone. *Journal of Geology* **103**, 95–105.

CRITELLI, S. & LE PERA, E. 1998. Post-Oligocene sediment dispersal systems and unroofing history of the Calabrian Microplate, Italy. *International Geology Review* **48**, 609–37.

CRITELLI, S., LE PERA, E., GALLUZZO, F., MILLI, S., MOSCATELLI, M., PERROTTA, S. & SANTANTONIO, M. 2007. Interpreting siliciclastic-carbonate detrital modes in foreland basin systems: an example from Upper Miocene arenites of the central Apennines, Italy. *Special Paper of the Geological Society of America* **420**, 107–33.

CRITELLI, S., MONGELLI, G., PERRI, F., MARTÌN-ALGARRA, A., MARTÌN-MARTÌN, M., PERRONE, V., DOMINICI, R., SONNINO, M. & ZAGHLOUL, M. N. 2008. Compositional and geochemical signatures for the sedimentary evolution of the Middle Triassic–Lower Jurassic continental redbeds from Western-Central Mediterranean Alpine Chains. *Journal of Geology* **116**, 375–86.

CRITELLI, S., MUTO, F., TRIPODI, V. & PERRI, F. 2011. Relationships between Lithospheric Flexure, Thrust Tectonics and Stratigraphic Sequences in Foreland Setting: the Southern Apennines Foreland Basin System, Italy. In *New Frontiers in Tectonic Research - At the Midst of Plate Convergence* (ed. U. Schattner), pp. 121–70. Rijeka, Croatia: InTech Open Access Publisher.

CRITELLI, S., MUTO, F., TRIPODI, V. & PERRI, F. 2013. Link between thrust tectonics and sedimentation processes of stratigraphic sequences from the southern Apennines foreland basin system, Italy. *Rendiconti Online della Società Geologica Italiana* **25**, 21–42.

CULLERS, R. L. 1994. The controls on the major and trace element variation of shales, siltstones, and sandstones of Pennsylvanian-Permian age from uplifted continental blocks in Colorado to platform sediments in Kansas, USA. *Geochimica et Cosmochimica Acta* **58**, 4955–72.

CULLERS, R. L. 2000. The geochemistry of shales, siltstones and sandstones of Pennsylvanian-Permian age,

Colorado, USA: implications for provenance and meta-morphic studies. *Lithos* **51**, 181–203.

CULLERS, R. L. 2002, Implications of elemental concentrations for provenance, redox conditions, and metamorphic studies of shales and limestones near Pueblo, CO, USA. *Chemical Geology* **191**, 305–27.

CULLERS, R. L. & PODKOVYROV, V. M. 2002. The source and origin of terrigenous sedimentary rocks in the Mesoproterozoic Ui group, southeastern Russia. *Precambrian Research* **117**, 1157–83.

DECIMA, A., MCKENZIE, J. A. & SCHREIBER, B. C. 1988. The origin of evaporative limestones: an example from the Messinian of Sicily (Italy). *Journal of Sedimentary Petrology* **58**, 256–72.

DESSAU, G., GONFI ANTINI, R. & TONGIORGI, E. 1959. L'origine dei giacimenti solfi feri italiani alla luce delle indagini isotopiche sui carbonati della serie gessoso solfi fera della Sicilia. *Bollettino del Servizio Geologico Italiano* **81**, 313–48.

DI STEFANO, A., VERDUCCI, M., LIRER, F., FERRARO, L., IACCARINO, S. M., HÜSING, S. K. & HILGEN, F. J. 2010. Paleoenvironmental conditions preceding the Messinian Salinity Crisis in the Central Mediterranean: integrated data from the Upper Miocene Trave section (Italy). *Palaeogeography, Palaeoclimatology, Palaeoecology* **297**, 37–53.

FAUQUETTE, S., SUC, J. P., BERTINI, A., POPESCU, S. M., WARNY, S., TAOUFIQ, N. B., PEREZ VILLA, M. G., CHIKHI, H., FEDDI, N., SUBALLY, D., CLAUZON, G. & FERRIER, J. 2006. How much did climate force the Messinian salinity crisis? Quantified climatic conditions from pollen records in the Mediterranean region. *Palaeogeography, Palaeoclimatology, Palaeoecology* **238**, 281–301.

FEDO, C. M., NESBITT, H. W. & YOUNG, G. M. 1995. Unravelling the effect of potassium metasomatism in sedimentary rocks and paleosols, with implications for paleoweathering conditions and provenance. *Geology* **23**, 921–4.

FRANZINI, M., LEONI, L. & SAITTA, M. 1972. A simple method to evaluate the matrix effects in X-ray fluorescence analysis. *X-Ray Spectrometry* **1**, 151–4.

GAETANI, G. A. & COHEN, A. L. 2006. Element partitioning during precipitation of aragonite from seawater: a framework for understanding paleoproxies. *Geochimica et Cosmochimica Acta* **70**, 4617–34.

GARCIA, D., COEHLO, J. & PERRIN, M. 1991 Fractionation between TiO2 and Zr as a measure of sorting within shale and sandstone series (northern Portugal). *European Journal of Mineralogy* **3**, 401–14.

GARCIA-VEIGAS, J., ORTI, F., ROSELL, L., AYORA, C., ROUCHY, J. M. & LUGLI, S. 1995. The Messinian salt of the Mediterranean: geochemical study of the salt from the Central Sicily Basin and comparison with the Lorca Basin (Spain). *Bulletin de la Societé géologique de France* **166**, 699–710.

GUIDO, A., JACOB, J., GAUTRET, P., LAGGOUN-DÉFARGE, F., MASTANDREA, A. & RUSSO, F. 2007. Molecular fossils and other organic markers as palaeoenvironmental indicators of the Messinian Calcare di Base Formation: normal versus stressed marine deposition (Rossano Basin, northern Calabria, Italy). *Palaeogeography, Palaeoclimatology, Palaeoecology* **255**, 265–83.

HARNOIS, L. 1988. The C.I.W. index: a new chemical index of weathering. *Sedimentary Geology* **55**, 319–22.

HSÜ, K. J., RYAN, W. B. F. & CITA, M. B. 1973. Late Miocene desiccation of the Mediterranean. *Nature* **242**, 240–4.

KRUMM, S. 1996. WINFIT 1.2: version of November 1996 (The Erlangen geological and mineralogical software collection) of "WINFIT 1.0: a public domain program for interactive profile-analysis under WINDOWS". XIII Conference on Clay Mineralogy and Petrology, Praha, 1994. *Acta Universitatis Carolinae Geologica* **38**, 253–61.

LACASSIE, J. P., HERVÈ, F. & ROSER, B. 2006. Sedimentary provenance study of the post-Early Permian to pre-Early Cretaceous metasedimentary Duque de York Complex, Chile. *Revista Geologica de Chile* **33**, 199–219.

LAND, L. S. 1980. The isotopic and trace element geochemistry of dolomite: the state of the art. In *Concepts and Models of Dolomitization* (eds D. H. Zenger, J. B. Dunham & R. L. Ethington), pp. 87–110. Society of Economic Paleontologists and Mineralogists Special Publication no. 28.

LAST, W. M. & GINN, F. W. 2005. Saline system of the Great Plains of western Canada: an overview of the limnogeology and paleolimnology. *Saline Systems* **1**, 1–38.

LEONI, L. & SAITTA, M. 1976. X-ray fluorescence analysis of 29 trace elements in rock and mineral standards. *Rendiconti Società Italiana di Mineralogia e Petrologia* **32**, 497–510.

LE PERA, E., ARRIBAS, J., CRITELLI, S. & TORTOSA, A. 2001. The effects of source rocks and chemical weathering on the petrogenesis of siliciclastic sand from the Neto River (Calabria, Italy): implications for provenance studies. *Sedimentology* **48**, 357–77.

LE PERA, E., CRITELLI, S. & SORRISO-VALVO, M. 2000. Weathering of gneiss in Calabria, Southern Italy. *Catena* **42**, 1–15.

LIU, Y. S., HU, Z. C., LI, M. & GAO, S. 2013. Applications of LA-ICP-MS in the elemental analyses of geological samples. *Chinese Science Bulletin* **58**, 3863–78.

MACHEL, H. G. & ANDERSON, J. H. 1989. Pervasive subsurface dolomitization of the Nisku Formation in central Alberta. *Journal of Sedimentary Petrology* **59**, 891–911.

MAHJOOR, A. S., KARIMI, M. & RASTEGARLARI, A. 2009 Mineralogical and geochemical characteristics of clay deposits from South Abarkouh district of clay deposit (Central Iran) and their applications. *Journal of Applied Sciences* **9**, 601–14.

MANZI, V., LUGLI, S., ROVERI, M., SCHREIBER, B. C. & GENNARI, R. 2010. The Messinian "Calcare di Base" (Sicily, Italy) revisited. *Geological Society of America Bulletin* **123**, 347–70.

MATSON, S. D. & FOX, D. L. 2010. Stable isotopic evidence for terrestrial latitudinal climate gradients in the Late Miocene of the Iberian Peninsula. *Palaeogeography, Palaeoclimatology, Palaeoecology* **287**, 28–44.

MCLENNAN, S. M., HEMMING, D. K. & HANSON, G. N. 1993. Geochemical approaches to sedimentation, provenance and tectonics. *Geological Society of America Special Papers* **284**, 21–40.

MCLENNAN, S. M., TAYLOR, S. R. & HEMMING, S. R. 2006. Composition, differentiation, and evolution of continental crust: constrains from sedimentary rocks and heat flow. In *Evolution and Differentiation of the Continental Crust* (eds M. Brown & T. Rushmer), pp. 92–134. Cambridge: Cambridge University Press.

MELAKU, S., WONDIMU, T., DAMS, R. & MOENS, L. 2004. Simultaneous determination of trace elements in Tinishu Akaki River water sample, Ethiopia, by ICP-MS. *Canadian Journal of Analytical Sciences and Spectroscopy* **49**, 374–84.

MONGELLI, G. 2004. Rare-earth elements in Oligo-Miocenic pelitic sediments from Lagonegro basin, southern Apennines, Italy: implications for provenance and source-area

weathering. *International Journal of Earth Sciences* **93**, 612–20.

MONGELLI, G., CRITELLI, S., PERRI, F., SONNINO, M. & PERRONE, V. 2006. Sedimentary recycling, provenance and paleoweathering from chemistry and mineralogy of Mesozoic continental redbed mudrocks, Peloritani Mountains, Southern Italy. *Geochemical Journal* **40**, 197–209.

MONGELLI, G., CULLERS, R. & MUELHEISEN, S. 1996. Geochemistry of Cenozoic shales from the Varicolori Formation, Southern Apennines, Italy: implications for mineralogical, grain size control and provenance. *European Journal of Mineralogy* **8**, 733–54.

MONGELLI, G., MAMELI, P., OGGIANO, G. & SINISI, R. 2012. Messinian palaeoclimate and palaeo-environment in the western Mediterranean realm: insights from the geochemistry of continental deposits of NW Sardinia (Italy). *International Geology Review* **54**, 971–90.

NESBITT, H. W., FEDO, C. M. & YOUNG, G. M. 1997. Quartz and feldspar stability, steady and non-steady-state weathering, and petrogenesis of siliciclastic sands and muds. *Journal of Geology* **105**, 173–91.

NESBITT, H. W. & YOUNG, G. M. 1982. Early Proterozoic climates and plate motions inferred from major element chemistry of lutites. *Nature* **299**, 715–7.

NESTEROFF, W. D. 1973. Un modèle pour les evaporates messiniennes en Méditerranée des bassins peu profonds avec depot d'evaporites lagunaires. In *Messinian Events in the Mediterranean* (ed. C. W. Drooger), pp. 68–81. Amsterdam: North-Holland Publishing Company.

OGNIBEN, L. 1955. Le argille scagliose del Crotonese. *Memorie e Note dell'Istituto di Geologia Applicata*. Napoli **6**, 1–72.

OGNIBEN, L. 1957. Petrografia della serie Solfigera Siciliana e considerazioni geologiche relative. *Memorie Descrittive della Carta Geologica d'Italia* **33**, 1.

OGNIBEN, L. 1962. Le Argille Scagliose e i sedimenti messiniani a sinistra del Trionto (Rossano, Cosenza). *Geologica Romana* **1**, 255–82.

OGNIBEN, L. 1969. Schema introduttivo alla geologia del confine calabro-lucano. *Memorie della Società Geologica Italiana* **8**, 453–763.

OHTA, T. & ARAI, H. 2007. Statistical empirical index of chemical weathering in igneous rocks: a new tool for evaluating the degree of weathering. *Chemical Geology* **240**, 280–97.

PATACCA, E., SARTORI, R. & SCANDONE, P. 1990. Tyrrhenian Basin and Apenninic arcs: kinematic relations since late Tortonian times. *Memorie della Società Geologica Italiana* **45**, 425–51.

PEDLEY, H. M. & GRASSO, M. 1993. Controls on faunal sediment cyclicity within the "Tripoli" and Calcare di Base basins (Late Miocene) of central Sicily. *Palaeogeography, Palaeoclimatology, Palaeoecology* **105**, 337–60.

PELTOLA, P., BRUN, C., STRÖM, M. & TOMILINA, O. 2008. High K/Rb ratios in stream waters – exploring plant litter decay, ground water and lithology as potential controlling mechanisms. *Chemical Geology* **257**, 92–100.

PERRI, F. 2014. Composition, provenance and source weathering of Mesozoic sandstones from Western-Central Mediterranean Alpine Chains. *Journal of African Earth Sciences* **91**, 32–43.

PERRI, F., CIRRINCIONE, R., CRITELLI, S., MAZZOLENI, P. & PAPPALARDO, A. 2008. Clay mineral assemblages and sandstone compositions of the Mesozoic Longobucco Group, northeastern Calabria: implications for burial history and diagenetic evolution. *International Geology Review* **50**, 1116–31.

PERRI, F., CRITELLI, S., CAVALCANTE, F., MONGELLI, G., DOMINICI, R., SONNINO, M. & DE ROSA, R. 2012*a*. Provenance signatures for the Miocene volcaniclastic succession of the Tufiti di Tusa Formation, southern Apennines, Italy. *Geological Magazine* **149**, 423–42.

PERRI, F., CRITELLI, S., DOMINICI, R., MUTO, F., TRIPODI, V. & CERAMICOLA, S. 2012*b*. Provenance and accommodation pathways of late Quaternary sediments in the deep-water northern Ionian Basin, southern Italy. *Sedimentary Geology* **280**, 244–59.

PERRI, F., CRITELLI, S., MARTÌN-ALGARRA, A., MARTÌN-MARTÌN, M., PERRONE, V., MONGELLI, G. & ZATTIN, M. 2013. Triassic redbeds in the Malaguide Complex (Betic Cordillera – Spain): petrography, geochemistry, and geodynamic implications. *Earth-Science Reviews* **117**, 1–28.

PERRI, F., CRITELLI, S., MONGELLI, G. & CULLERS, R. L. 2011. Sedimentary evolution of the Mesozoic continental redbeds using geochemical and mineralogical tools: the case of Upper Triassic to Lowermost Jurassic M.te di Gioiosa mudstones (Sicily, southern Italy). *International Journal of Earth Sciences* **100**, 1569–87.

PERRI, F., MUTO, F. & BELVISO, C. 2011. Links between composition and provenance of Mesozoic siliciclastic sediments from Western Calabria (Southern Italy). *Italian Journal of Geosciences* **130**, 318–29.

PLANK, T. & LANGMUIR, C. H. 1998. The chemical composition of subducting sediment and its composition for the crust and mantle: *Chemical Geology* **145**, 325–94.

RODA, C. 1964. Distribuzione e facies dei sedimenti neogenici nel Bacino Crotonese. *Geologica Romana* **3**, 319–66.

RODA, C. 1967. I sedimenti neogenici autoctoni ed alloctoni della zona di Cirò-Cariati (Catanzaro e Cosenza). *Memorie della Società Geologica Italiana* **6**, 137–49.

ROUCHY, J. M. & CARUSO, A. 2006. The Messinian salinity crisis in the Mediterranean basin: a reassessment of the data and an integrated scenario. *Sedimentary Geology* **188–189**, 35–67.

ROVERI, M., LUGLI, S., MANZI, V. & SCHREIBER, B. C. 2008*a*. The Messinian Sicilian stratigraphy revisited: new insights for the Messinian salinity crisis. *Terra Nova* **20**, 483–8.

ROVERI, M., MANZI, V., GENNARI, R., IACCARINO, S. M. & LUGLI, S. 2008*b*. Recent advancements in the Messinian stratigraphy of Italy and their Mediterranean-scale implications. *Bollettino della Società Paleontologica Italiana* **47**, 71–85.

SALMINEN, R., BATISTA, M. J., BIDOVEC, M., DEMETRIADES, A., DE VIVO, B., DE VOS, W., DURIS, M., GILUSIS, A., GREGORAUSKIENE, V., HALAMIC, J., HEITZMANN, P., LIMA, A., JORDAN, G., KLAVER, G., KLEIN, P., LIS, J., LOCATURA, J., MARSINA, K., MAZREKU, A., O'CONNNOR, P. J., OLSSON, S. A., OTTEEN, R.-T., PETERSELL, V., PLANT, J. A., REEDER, S., SALPETEUR, I., SANDSTROM, H., SIWERS, U., STEENFELT, A. & TARVAINEN, T. 2005. *Geochemical Atlas of Europe. Part 1: Background Information, Methodology and Maps*. Espoo, Finland: Geological Survey of Finland, 526 pp.

SÁNCHEZ-ROMÁN, M., MCKENZIE, J. A., DE LUCA REBELLO WAGENER, A., RIVADENEYRA, M. A. & VASCONCELOS, C. 2009. Presence of sulfate does not inhibit low-temperature dolomite precipitation. *Earth and Planetary Science Letters* **285**, 131–9.

SELLI, R. 1973. An outline of the Italian Messinian. In *Messinian Events in the Mediterranean* (ed. C. W. Drooger), pp. 150–70. Amsterdam: North-Holland Publishing Company.

TAYLOR, S. R. & MCLENNAN, S. M. 1985. *The Continental Crust: Its Composition and Evolution*. Oxford: Blackwell.

THOMSON, J., CRUDELI, D., DE LANGE, G. J., SLOMP, C., ERBA, E. & CORSELLI, C. 2004. Florisphaera profunda and the origin and diagenesis of carbonate phases in eastern Mediterranean sapropel units. *Paleoceanography* **19**, PA3003.

TRIPODI, V., MUTO, F. & CRITELLI, S. 2013. Structural style and tectono-stratigraphic evolution of the Neogene-Quaternary Siderno Basin, southern Calabrian Arc, Italy. *International Geology Review* **55**, 468–81.

VAN DIJK, J. P., BELLO, M., BRANCALEONI, G. P., CANTARELLA, G., COSTA, V., FRIXA, A., GOLFETTO, F., MERLINI, F., RIVA, M., TORRICELLI, S., TOSCANO, C. & ZERILLI, A. 2000. A regional structural model for the northern sector of the Calabrian Arc (southern Italy). *Tectonophysics* **324**, 23–60.

WRAFTER, J. P. & GRAHAM, J. R. 1989. Ophiolitic detritus in the Ordovician sediments of South Mayo Ireland. *Journal of the Geological Society, London* **146**, 213–5.

WRONKIEWICZ, D. J. & CONDIE, K. C. 1989. Geochemistry and provenance of sediments from the Pongola Supergroup, South Africa: evidence for a 3.0 Ga old continental craton. *Geochimica et Cosmochimica Acta* **53**, 1537–49.

ZAGHLOUL, M. N., CRITELLI, S., PERRI, F., MONGELLI, G., PERRONE, V., SONNINO, M., TUCKER, M., AIELLO, M. & VENTIMIGLIA, C. 2010. Depositional systems, composition and geochemistry of Triassic rifted-continental margin redbeds of Internal Rif Chain, Morocco. *Sedimentology* **57**, 312–50.

ZECCHIN, M., CAFFAU, M., CIVILE, D., CRITELLI, S., DI STEFANO, A., MANISCALCO, R., MUTO, F., STURIALE, G. & RODA, C. 2012. The Plio-Pleistocene evolution of the Crotone Basin (southern Italy): interplay between sedimentation, tectonics and eustasy in the frame of Calabrian Arc migration. *Earth-Science Reviews* **115**, 273–303.

ZECCHIN, M., CERAMICOLA, S., GORDINI, E., DEPONTE, M. & CRITELLI, S. 2011. Cliff overstep model and variability in the geometry of transgressive erosional surfaces in high-gradient shelves: the case of the Ionian Calabrian margin (southern Italy). *Marine Geology* **281**, 43–58.

ZECCHIN, M., CIVILE, D., CAFFAU, M., MUTO, F., DI STEFANO, A., MANISCALCO, R., CRITELLI, S. 2013a. The Messinian succession of the Crotone Basin (southern Italy) I: stratigraphic architecture reconstructed by seismic and well data. *Marine and Petroleum Geology* **48**, 455–73.

ZECCHIN, M., CAFFAU, M., DI STEFANO, A., MANISCALCO, R., LENAZ, D., CIVILE, D., MUTO, F. & CRITELLI, S. 2013b. The Messinian succession of the Crotone Basin (southern Italy) II: Facies architecture and stratal surfaces across the Miocene-Pliocene boundary. *Marine and Petroleum Geology* **48**, 474–92.